Arabian Journal of Chemistry 16 (2023) 105254

Contents lists available at ScienceDirect

Arabian Journal of Chemistry

journal homepage: www.sciencedirect.com

Original article

Low-cost and eco-friendly biosorbent for effective removal of hazardous ions from simulated radioactive liquid waste

Sayed S. Metwally [a,*], Emad H. Borai [a], Mostafa M. Hamed [a], Tarek M. Mohamed [b], Mahmoud G. Hamed [a], Walaa R. Mohamed [a]

[a] Egyptian Atomic Energy Authority, Hot Laboratories and Waste Management Center, 13759 Cairo, Egypt
[b] Egyptian Atomic Energy Authority, National Centre for Radiation Research and Technology, Cairo, Egypt

ARTICLE INFO

Article history:
Received 30 March 2023
Accepted 6 September 2023
Available online 11 September 2023

Keywords:
Biosorbent
Radioactive waste
Kinetics
Isotherm

ABSTRACT

Rice bran (RB) is distinguished by its chemical stability, insoluble in water, and local availability, in addition to the presence of ionizable functional groups which able to bind with the elements. Hence, this material was preferred to be utilized in this study as an operative biosorbent of altered hazardous ions such as Pb^{2+}, Sr^{2+}, and Eu^{3+} from simulated radioactive waste to attain a safe environment free from the risk of such waste. The kinetic studies illustrated that the sorption process obeys the pseudo-second-order model. From the isotherm studies, Langmuir is the most applicable isotherm model to the experimental data with monolayer sorption capacities of 1.26, 0.76, and 0.33 mmol/g for Sr^{2+}, Eu^{3+}, and Pb^{2+}, respectively. The efficiency of RB was evaluated by applying it to a simulated radioactive waste containing multicomponent to study the interfering ions. When the sorption capacities of RB and other sorbents were compared, it became clear that RB had a significantly higher sorption capacity than most sorbents. The findings exposed that RB is a material with the potential for the treatment of radioactive waste and can be successfully applied in this regard.

1. Introduction

Everyone wishes to live in a safe and healthy environment and the world unites for a clean and hazard-free environment. Therefore, most researchers are interested in solving the problem of increasing the volume of radioactive waste caused by a rise in peaceful nuclear activity.

In the literature review, there are altered approaches employed to treat the liquid radioactive waste such as adsorption (Kitikova et al., 2017), exchange (Ivanets et al., 2014), impregnation (Ibrahim et al., 2021), biosorption (Metwally et al., 2017), immobilization (Panasenko et al., 2022), and fixed-bed column (Sami et al., 2022). Also, there are numerous sorbent materials utilized in the field of liquid waste treatment as metal oxides (Ahmed et al., 2020), composite polymers (El-Masry et al., 2023), activated carbon (Makarov et al., 2021), and hydroxide sludge (Hamed et al., 2019a). The biosorption procedure attracted the attention of several researchers since it is economic method and has less health risk than the current procedures. Therefore, this work has concerned with desiring the biosorption method to remove some ions from solutions utilizing low-cost and eco-friendly biosorbent material which is rice bran (RB). Rice bran is the upper layer of rice and produced from rice milling process as a by-product, it contains different polymers as polysaccharides (cellulose and starch), phenolic and phytic acids; cellulose has a high degree of polymerization and is considered as a long-chain homopolymer (Zhuang et al., 2019; Mohamed et al., 2022a,b). Due to the major prominence of the exclusive RB composition, its components are extracted to be utilized in operative form since they have numerous function groups as carboxyl, hydroxyl, and amine groups which are influential in the sorption processes. RB is distinguished by its chemical stability, insoluble in water, and local availability, also, the existence of ionizable functional groups which able to bind with the elements (Montanher et al., 2005). Hence, this material was preferred to be utilized in this study as an operative biosorbent of altered hazardous ions from simulated radioactive liquid waste.

It is well known that stable and radioactive elements behave similarly chemically under the same conditions. However, it is cru-

* Corresponding author.
E-mail address: sicosad@hotmail.com (S.S. Metwally).
Peer review under responsibility of King Saud University.

Production and hosting by Elsevier

https://doi.org/10.1016/j.arabjc.2023.105254
1878-5352/

cial to remember that the concentration of different ions in solution can has a major impact on how they behave in sorption processes. Therefore, the sorption of stable ions is different from radionuclides due to the difference in their concentrations (Ivanets et al., 2020).

Heavy metals including nickel, strontium, lead, cadmium, and europium are abundant in radioactive and industrial liquid wastes, which can have detrimental effects on the environment if they are not properly managed. The biological machinery of organisms may be irreparably harmed by the bioaccumulation of these contaminants. As a result, they ought to be given a secure setting. Lead owns different isotopes including ^{210}Pb which has a half-life of 22.3 years; it produces both α-particles and γ-radiation (Weng et al., 2020). The original source of ^{210}Pb is the ^{238}U decay chain, which occurs naturally (Sami et al., 2022). Since ^{210}Pb is diffused in the air, water, and soil, its buildup may endanger human health by increasing the risk of cancer, destroying kidney, and have a negative influence on the ecosystem (Ghaly et al., 2018). Wastewater treatment before release into the environment is the crucial step in the anticipation of lead contamination. As a result, the removal

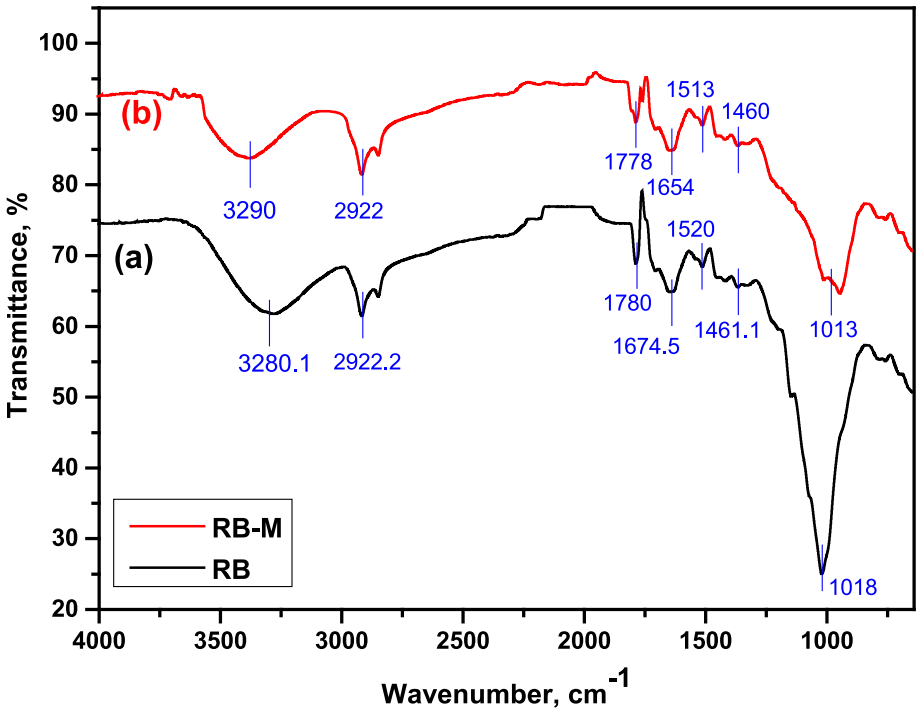

Fig. 1. FT-IR Spectra of (a) RB before the sorption and (b) RB-M after the sorption.

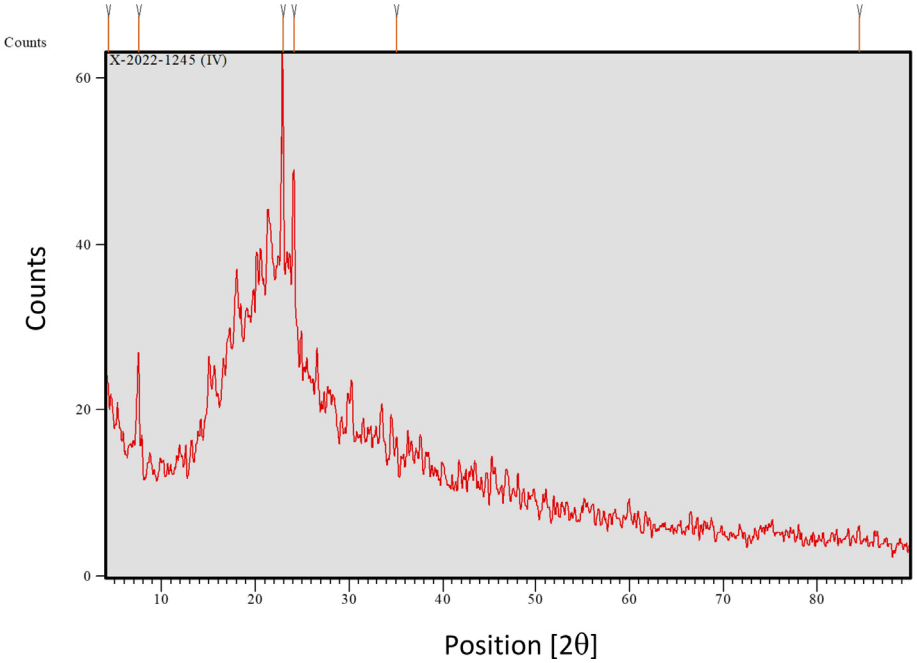

Fig. 2. XRD pattern of the biosorbent material.

of Pb^{2+} from wastewater is particularly significant. The maximum allowable lead restriction is 10 ppb, and zero lead centralization of water is beneficial, according to WHO guidelines (Naga Babu et al., 2017).

The development of High-Tech devices is strongly increasing the demand for rare earth elements (Wei et al., 2021). The global production of lanthanides raises 167 tons in 2018 compared to 124 tons in 2010 (USEPA, 2012; and El-Masry et al., 2023). Lan-

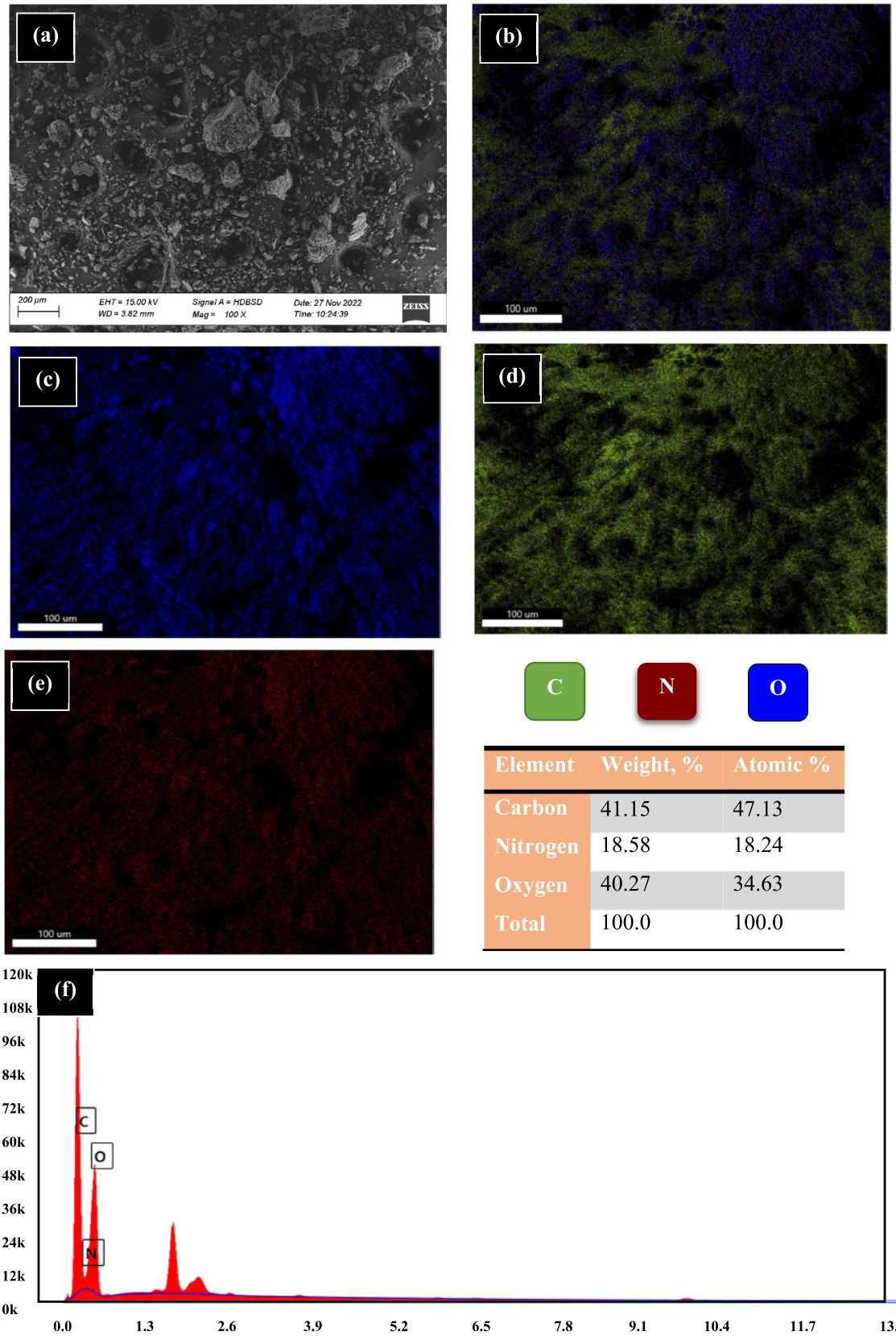

Element	Weight, %	Atomic %
Carbon	41.15	47.13
Nitrogen	18.58	18.24
Oxygen	40.27	34.63
Total	100.0	100.0

Fig. 3. RB before the sorption using SEM and EDX mapping.

thanides have a positive economic impact but their growing use in a variety of applications has also increased the amount of waste they produce. According to toxicological studies, lanthanides have a significant negative effect on organisms (Metwally et al., 2018). Europium is a representative element for lanthanides; 152 + 154Eu is a fission product that can also be produced by control rods when neutrons are activated. Thus, it is crucial to economically and environmentally recover lanthanides from industrial and radioactive waste.

Strontium isotope, ^{90}Sr, should be removed from radioactive waste since it is highly soluble, bioavailable and has a half-life of 28.8 years (Metwally et al., 2017). The biogeochemical features of strontium and calcium are very similar; both are alkaline earth metals with similar ionic radii (Shujun et al., 2015). Because of this similarity, strontium ions can exchange calcium in bone (Hamed et al., 2019b), which leads to leukaemia, bone cancer, and other cancers of the soft tissues when ingested. Therefore, removing strontium ions is very important.

Hence, this work concerned with utilizing an economical technique and efficient material for strontium, lead, and europium ions removal from simulated radioactive waste.

2. Materials and methods

2.1. Chemicals

Europium, lead, and strontium chlorides were supplied from Sigma-Aldrich. In order to create a stock solution, a specific amount of Eu^{3+}, Pb^{2+}, and Sr^{2+} were dissolved in bidistilled water. This solution had 1000 mg/L of each ion. Fluka-derived NH_4OH and/or HCl

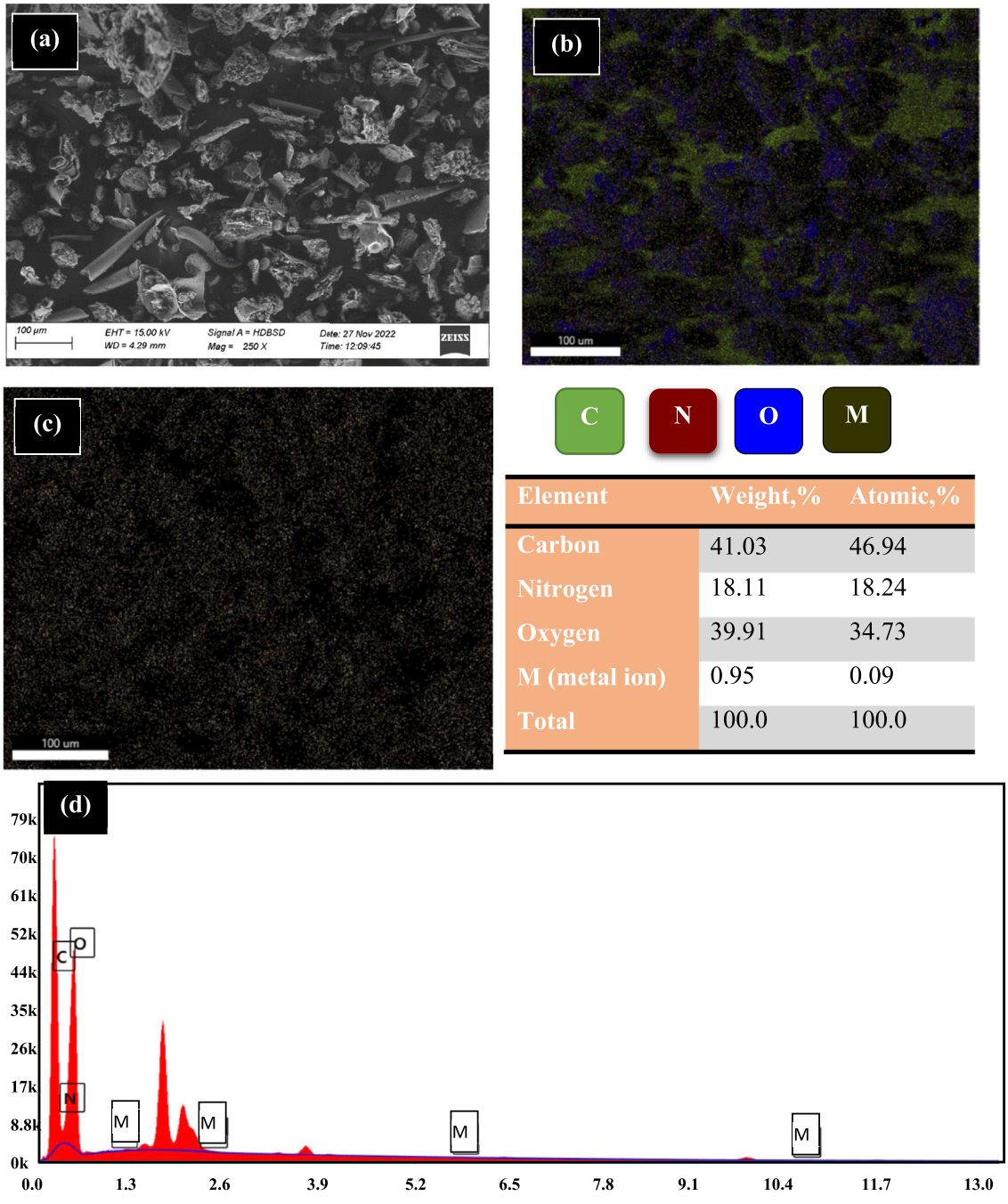

Element	Weight,%	Atomic,%
Carbon	41.03	46.94
Nitrogen	18.11	18.24
Oxygen	39.91	34.73
M (metal ion)	0.95	0.09
Total	100.0	100.0

Fig. 4. RB after the sorption using SEM and EDX mapping.

were used to change pH of the medium. Nitric acid, phosphoric acid, hydrochloric acid, and sulfuric acid were bought from Merck. As an industrial by-product, rice bran (RB) was gained from Egyptian rice mill manufacturers as an industrial waste. Bidistilled water was utilized for sample preparation and dilution in all studies.

2.2. Modification of rice bran

To remove the tissues and exclude foreign components, rice bran was sieved before being ground, cleaned, and dried at 70 °C. Then, one liter of 3% phosphoric acid was combined with 50 g of dried RB, and the mixture was agitated at 50 °C for two hours. The combination was filtered to separate the two phases after this time, and it was then allowed for 24 h to produce a fine grayish-white yield. After washing, the product was dried for 24 h at 60 °C. This procedure was repeated with several solvents, such as nitric, sulfuric, and hydrochloric acids. The results illustrated that phosphoric acid is the best solvent because it yields large amount of the product and the product is easily handled since it is not wetted. Hence, the modified sample by phosphoric acid was selected and irradiated with different doses (10–30 kGy) with dose rate 1.15 kGy/h of gamma rays at NCRRT, Cairo, Egypt, then the final product was washed several times by acetone, dried in an oven at 50 °C, and grinded producing RB with different particle sizes.

2.3. Characterization of the biosorbent material

The physicochemical features of the modified and irradiated rice bran (RB) were investigated utilizing altered techniques. The bonds and functional groups in the BR, before and after the sorption of metal ions, were detected by FT-IR (ALPHA II, Bruker, Germany). The surface morphology of the biosorbent material and the elemental analysis were displayed by Scanning Electron Microscope with EDX-mapping of Zeiss SmartEDX, Germany. Also, the crystallinity of the RB was examined by X-ray Diffraction using PANalytical (Netherland) Model: X'PertPRO (MPD).

2.4. Determination of point of zero charge

The pH level at which the net charge on the BR surface is zero is known as the point of zero charge (pH_{PZC}). It was computed using a series of 50 mL bottles having 0.1 g of RB and 10 mL of an electrolyte with a concentration of 0.1 mol/L, such as KNO_3. The mixture was agitated for an overnight period at various starting pH values between 1 and 10, $pH_{initial}$, at room temperature. The final pH, pH_{final}, of KNO_3 were detected in each case following centrifugation of the two phases.

2.5. Sorption investigations

2.5.1. Impact of pH

It was determined how Sr^{2+}, Pb^{2+}, and Eu^{3+} were sorbed by RB as a function of pH while maintaining other parameters. A series of bottles providing with 10 mL of a 10^{-3} mol/L ion and 0.1 g of RB were stirred overnight to ensure that the equilibrium was attained at room temperature before the pH value was determined. The initial pH of the solutions was changed to values between 1.0 and 6.0. At 5000 rpm, the mixture was centrifuged. Flame Atomic Absorption spectroscopy was used to measure the concentration of each ion in the clear aqueous phases, and the following equation is used to compute the % uptake.

$$Uptake, \% = \frac{C_o - C_e}{C_o} \times 100 \quad (1)$$

The initial and equilibrium ion concentrations, expressed in mol/L, are respectively C_e and C_o. Eq. (2) was employed to compute the ions distribution coefficient (K_d, mL/g).

$$K_d = \frac{C_o - C_e}{C_e} \times \frac{V}{m} \quad (2)$$

where V and m, respectively, stand for the sample volume in millilitres (mL) and the sorbent's mass in games.

2.5.2. Kinetic studies

The batch was carried out by agitating 0.1 g of RB with 10 mL of 10^{-3} mol/L of Sr^{2+}, Pb^{2+}, and/or Eu^{3+} at various interval durations (3–180 min) and pH 5.0 (the optimum pH value) to evaluate the sorption kinetics. Following the division of the two phases, the supernatant was utilized to measure each ion's concentration. It was determined how much was sorbed (q_t, mg/g).

$$q_t = (C_o - C_t) \times \frac{V}{m} \quad (3)$$

2.5.3. Equilibrium isotherm studies

Ion concentrations ranging from 2.5×10^{-2} to 5×10^{-5} mol/L were employed to investigate the ions' isotherm on RB. In a set of vials containing 10 mL of strontium, lead, and/or europium ions, 0.1 g of RB was put. After adjusting the pH to the optimum level, the mixture was stirred all night. Each ion's concentration in the filtrate was detected. The same equation, with C_t replaced by C_e (concentration of the ions at equilibrium) was utilized to compute the amount of ions that were sorbed at equilibrium (q_e, mg/g).

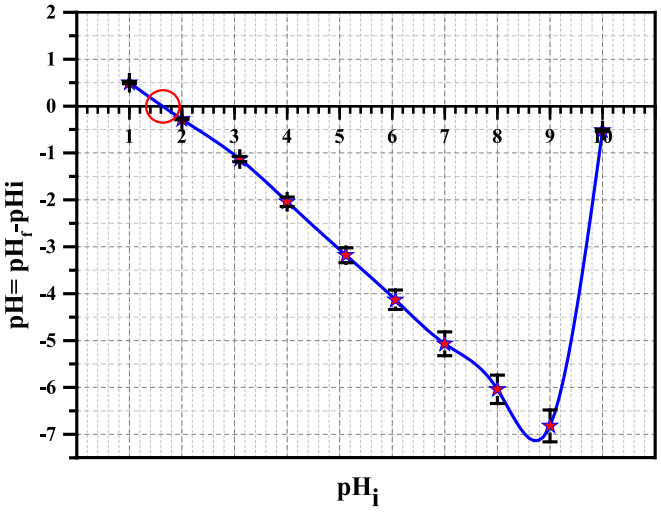

Fig. 5. Establishing the RB's zero point charge.

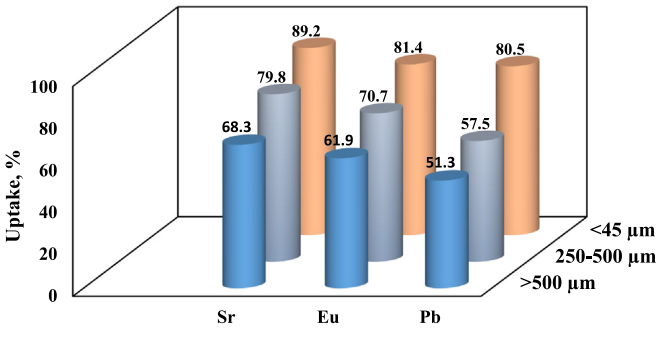

Fig. 6. Impact of RB particle size for sorption of Sr^{2+}, Eu^{3+}, and Pb^{2+}.

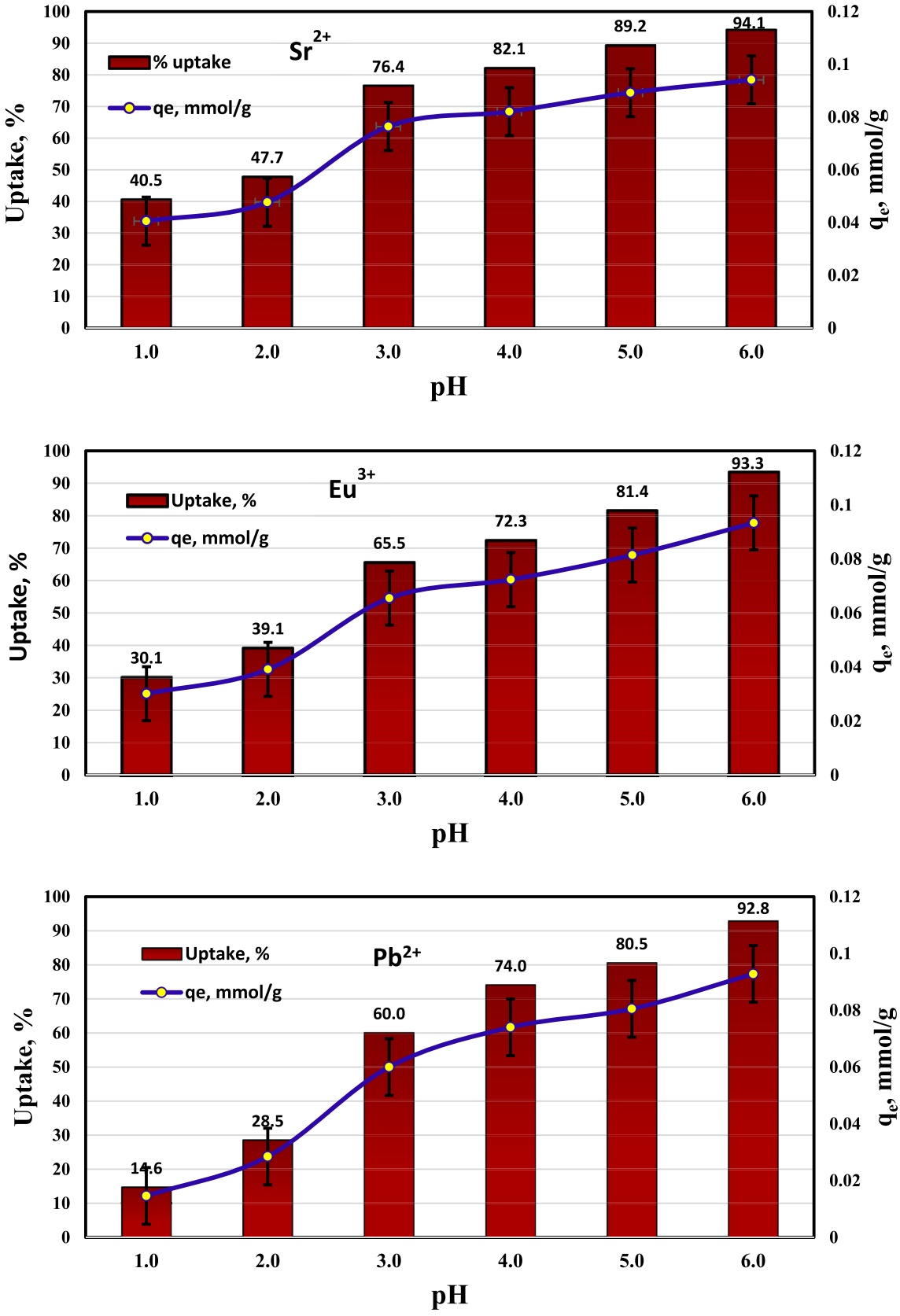

Fig. 7. Impact of pH on sorption of 10^{-3} mol/L Sr^{2+}, Pb^{2+}, and Eu^{3+} by RB.

2.6. Application of RB on simulated radioactive waste

Multicomponent solutions comprising various ions, including Sr^{2+}, Eu^{3+}, Pb^{2+}, Cs^{+}, Zn^{2+}, Co^{2+}, and Ni^{2+}, were used to investigate the sorption effectiveness of RB in a waste. For equilibrium time, a 10 mL sample solution (simulated waste) containing 0.2 g of RB was shaken at pH 5.0. The filtrate was examined to determine the ion concentrations after the separation of the two phases. The removal percentage was computed using Eq. (1).

3. Results and discussion

3.1. Characterization of the biosorbent

Fig. 1 displays the RB's FT-IR spectra both before and after the sorption. The four distinct functional groups (NH_2, C═O, OH, and COOH groups) are present, as exposed in the spectra, and they are as follows;

According to Fig. 1(a), the broad band, which was observed between 3600 and 3000 cm^{-1} and centered at 3280.1 cm^{-1}, was attributed to the —OH stretching vibrations of polymeric compounds made of alcohols, phenols, and carboxylic acids. The band shifting suggests that the metal ions and —OH groups interact strongly, as revealed in Fig. 1(b). Stretching vibration of C—H aliphatic groups is attributed to the band at 2922.2 cm^{-1}. Carboxylate groups are thought to be responsible for the small band at 1461.1 cm^{-1}, which is supported by bands at 1780 cm^{-1}, Fig. 1 (a). These bands' shift and change in intensity also point to the sorption of ions, as displayed in Fig. 1(b). The amino group is appeared at around 1700–1650 cm^{-1} (Montanher et al., 2005). The band at 1674 cm^{-1} allows us to observe the ketonic and aldehydic C═O groups. The —OH bending of the adsorbed water is what causes the band to be around 1520.8 cm^{-1}. The phosphate group is indicated by the absorption band at 1018 cm^{-1}.

The XRD pattern of RB is illustrated in Fig. 2. As mentioned in the introduction section, the RB is mainly composed of cellulose; this is confirmed by obtaining a strong peak at $2\theta = 22.9°$ which is attributed to the crystals of cellulose (Zhao et al., 2022). Also, the peak at $2\theta = 24.1°$ confirms the crystalline structure of RB.

The morphological structure of RB was analyzed before and after the sorption by SEM with EDX-mapping as displayed in Figs. 3 and 4, respectively. The images expose visibly multi-hole structures with altered diameters for RB before the sorption and the existence of pellets, Fig. 3(a). The multi-hole structure is due to the presence of cellulose molecules, this is consistent with the available literature (Qinglan et al., 2021; Qu et al., 2019). These cavities are helpful for capturing the ions where the active sites are easily exposed. Fig. 3(b, c, d, and e) displays that RB is principally made up of O, C, and N atoms. This was confirmed by EDX (Fig. 3(f)) that establishes the presence of atoms; the most prevalent element with weight percentage of 41.15% is carbon atom, while nitrogen and oxygen atoms are existing with 18.58 and 40.27%, respectively. After the sorption, the hole structure was disappeared since the holes are occupied by the sorbed ions and a rougher surface was obtained. Fig. 4 shows the spectroscopic evidence for presence of ions sorbed by RB.

3.2. Effect of irradiation dose on the rice bran

Irradiation of raw materials such as rice bran that include different types of natural polymers as cellulose (carboxymethylcellulose) is carried out to reduce molecular weight and particle size of the material (IAEA, 2009). Decreasing the particle size leads to increase the surface area, hence, the material's efficiency in the sorption process is increased. The data gained to determine the effect of different doses of irradiation indicated that the yield of rice bran increased from 22 to 35 g/kg as the irradiation dose increased from 0 to 30 kGy. Therefore, the optimum irradiation dose was desired at 30 kGy.

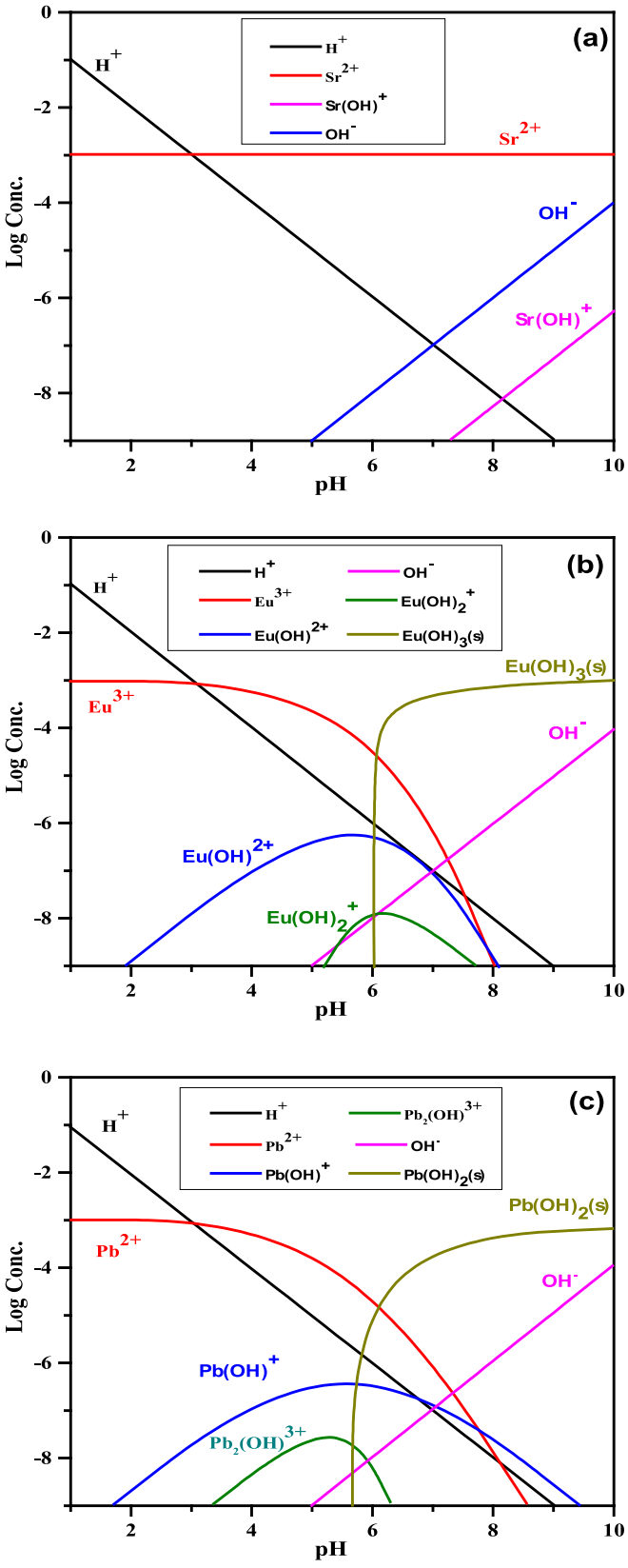

Fig. 8. Speciation of (a) strontium, (b) europium, and (c) lead at different pH values.

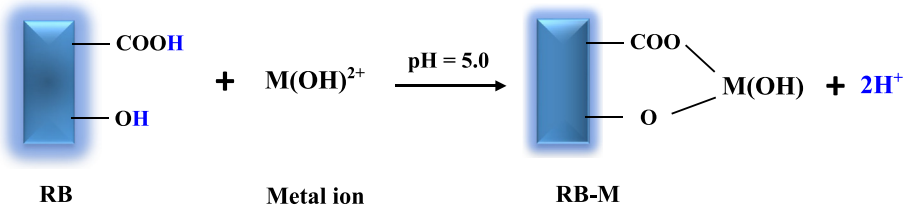

Scheme 1. Mechanism for sorption of metal ions on RB.

3.3. Establishing the RB's zero point charge

By estimating the Zero Point Charge value (pH_{ZPC}), it was possible to determine the surface charge of RB. The term "Zero Point Charge" refers to the pH level at which the surface of substance has a neutral charge (zero charge), with negative charges present above and positive charges present below. Plotting the initial value of pH ($pH_{initial}$) against ΔpH (pH_{final}-$pH_{initial}$), as exposed in Fig. 5. It was discovered that the pH_{ZPC} was 1.6. Thus, at pH > 1.6, the RB surface has negative charge, increasing the material's capacity to bind cations throughout a range of pH.

3.4. Impact of RB particle size

Particle size impact of sorbents is very significant to state the best appropriate size for optimizing the sorption investigation.

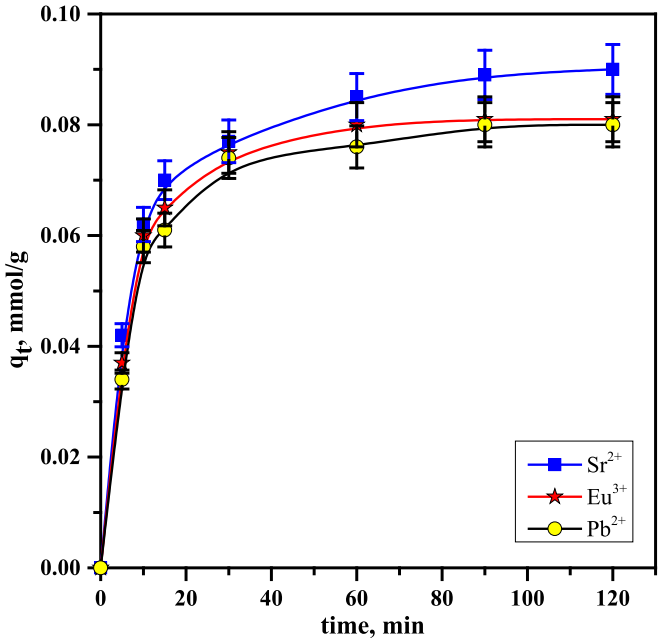

Fig. 9. Impact of contact time on the sorption of 10^{-3}mol/L Sr^{2+}, Pb^{2+}, and Eu^{3+} using RB.

Fig. 6 presents the influence of particle size of the modified rice barn (RB) on removal of Sr^{2+}, Eu^{3+}, and Pb^{2+}; the findings demonstrated that as the RB particle size decreased the ions removal increased, to promote ion diffusion through the sorbent and lower the mass transfer resistance for the sorption, the surface area of RB is increased with decreasing its particle size. Hence, the smallest particle size (<45 μm) was preferred as the optimum particle size.

3.5. Impact of pH and speciation

Since hydroxyl and hydrogen ions actively compete with other ions during the sorption process, the pH is the most important factor controlling the ions' diffusion on sorbents. The sorption properties maybe affected by the pH via a number of mechanisms including; the metal precipitation (at the highest pH values), the speciation of the metal, or the overall charge of the sorbent (Elwakeel et al., 2021). At pH range 1.0–6.0, the pH impact on the elimination of Sr^{2+}, Pb^{2+}, and Eu^{3+} was employed. In order to stop the ions from precipitating, higher pH values were avoided. The percent uptake and the distribution coefficient of the ions were computed by Eqs. (1) and (2). The results established that the percent uptake rises by raising the pH value. According to Fig. 7, the ideal pH for the three cations was determined to be pH 5.0, where the percentage uptake for Sr^{2+}, Pb^{2+}, and Eu^{3+}, respectively, was found 89.2, 80.5, and 81.4%.

As displayed in Fig. 8, the MEDUSA program, which offers details on the distribution of species at altered pH levels (Metwally et al., 2018), was utilized to estimate the species of strontium, lead, and europium in the liquid phase as a function of pH and concentration. Strontium is sorbed as Sr^{2+} since it is a free cation at all pH ranges (1.0–10.0), according to Fig. 8(a). As displayed in Fig. 8(c), distinct species of lead exist at pH values ranging from 1.0 to 10.0; at pH 5.0, lead exists in two species: free cations (Pb^{2+}) and hydrolyzed cations ($Pb(OH)^{+}$). The hydrolyzed cations are preferred to be sorbed on the solid material because it is known that they are more hydrophobic than free ions (Mohamed et al., 2022b). At higher pH values, lead is precipitated as $Pb(OH)_2$. Lead is consequently sorbed as $Pb(OH)^{+}$. As exposed in Fig. 8(b), the hydrolysis of europium results in changed species such Eu^{3+}, $Eu(OH)^{2+}$, $Eu(OH)_2^{+}$, $Eu(OH)_3$, and $Eu(OH)_4^{-}$. As the pH rises, numerous hydroxocomplexes would start to be produced through precipitation and hydrolysis. Europium occurs as trivalent cations, Eu^{3+}, and divalent complexes, $Eu(OH)^{2+}$, throughout the pH range investigated (1.0 to 6.0), especially at the ideal pH level (pH

Table 1
Parameters of kinetic models for sorption of Sr^{2+}, Eu^{3+}, and Pb^{2+} by RB at room temperature and pH = 5.0.

Pseudo-first-order					Pseudo-second-order		
ions	k_1, min^{-1}	$q_{e(Calc)}$, mmol/g	$q_{e(Exp)}$, mmol/g	R^2	k_2, g/mmol.min	$q_{e(Calc)}$, mmol/g	R^2
Sr^{2+}	0.039	0.047	0.09	0.97	1.8	0.094	0.99
Eu^{3+}	0.018	0.0372	0.081	0.76	2.28	0.086	0.99
Pb^{2+}	0.017	0.041	0.080	0.76	2.01	0.085	0.99

5.0), but outside of this range, it is precipitated as hydroxides, $Eu(OH)_3$. Europium was consequently sorbed as $Eu(OH)^{2+}$.

3.6. Proposed sorption mechanism

The hydrated ions ($Pb(OH)^+$ and $Eu(OH)^{2+}$) are favarable for sorption because, as previously noted, they are more hydrophobic than the free ions, dehydrate more readily, and adhere to the RB surface. This is consistent with the findings in the literature (Metwally et al., 2018). As stated in the introduction, RB comprises a number of function groups, including carboxyl, hydroxyl, carbonyl, and amine groups, which are supported by FT-IR spectra. The carboxyl and hydroxyl are more acidic groups than amine and carbonyl groups so they can release the hydrogen ions easly. Hence, they have exchangeable hydrogen ions;

The sorption mechanism can be proposed by replacing the metal ions with the hydrogen from the hydroxyl and carboxylic groups in RB, Scheme 1. As a result, they have exchangeable hydrogen ions. This was verified by estimating the pH following the sorption, which fell as a result of protons being released in the liquid phase. As divalent cations, Sr^{2+} and $Eu(OH)^{2+}$ were sorbed by exchanging two hydrogen ions. While only one hydrogen ion from the carboxyl group, which is more acidic than the hydroxyl group, was exchanged to sorb $Pb(OH)^+$.

3.7. Impact of contact time

Fig. 9 demonstrates that as the time passes, the RB's sorption of Sr^{2+}, Eu^{3+}, and Pb^{2+} increases. Using Eq. (3) to compute the amount sorbed, the results illustrated that the quantity gradually increased until attaining equilibrium at 0.09, 0.081, and 0.08 mol/g for Sr^{2+}, Eu^{3+}, and Pb^{2+}, respectively. The initial sorption rate is high, and it gradually declines as the available sorption sites are exhausted and the thickness of the border layer rises. For the three ions, the equilibrium time was attained after 90 min. The following kinetic models were applied. The equilibrium time was reached after 90 min for the three ions. Some kinetic models were used as follows.

3.7.1. Pseudo-first-order model

For the sorption of the three ions by RB, kinetic models as pseudo-first- and pseudo-second-order models were employed. For the pseudo-first-order, the difference between the starting and equilibrium ions concentrations is used to calculate the sorption rate. The Lagergren equation gives the following as the linear form.

$$\log(q_e - q_t) = \log q_e - \left(\frac{k_1}{2.303}\right)t \quad (4)$$

where k_1 refers to the constant sorption rate. The value of k_1 may be computed from the slope of the log(qe-qt) vs. t plot, whereas values for the theoretical quantity sorbed, $q_{e(Calc)}$, can be estimated from the intercept, as explored in Fig. S1(a), Supplementary Material. Table 1 lists the values for k_1 and q_e. The pseudo-first-order model is not relevant for sorption of Sr^{2+}, Eu^{3+}, and Pb^{2+} by RB, as shown by the table, which shows that there is a clear difference between the experimental and estimated q_e values.

3.7.2. Pseudo-second-order model

According to the pseudo-second-order, chemisorption demanding electron valency force or electron replace between sorbate and sorbent could be the reaction's rate-determining phase. Eq. (5) serves as a formula for this model.

$$\frac{t}{q_t} = \frac{1}{k_2 q_e^2} + \frac{1}{q_e}\, t \quad (5)$$

The rate constant, k_2, and the quantity of ions sorbed, q_e, can be estimated from the intercept and slope of the straight lines obtained by plotting t/q_t vs. t (Fig. S1(b), Supplementary Material). High val-

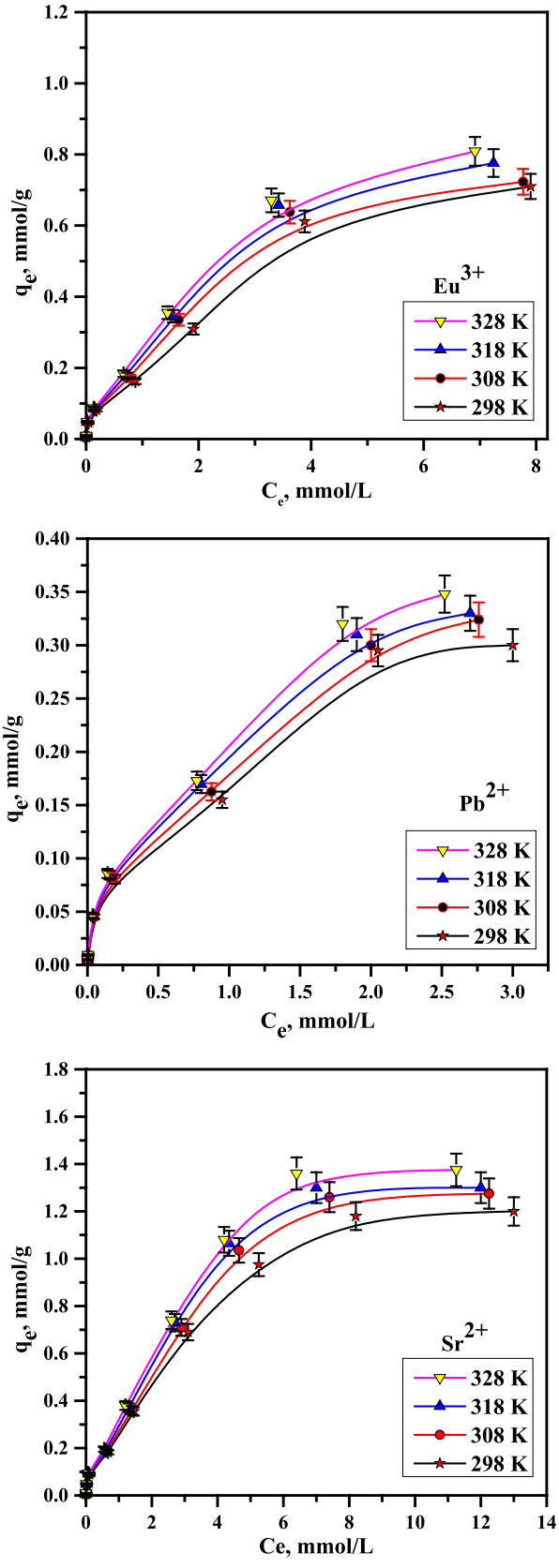

Fig. 10. Isotherm plot of Sr^{2+}, Pb^{2+}, and Eu^{3+} using RB.

Table 2
Parameters of Langmuir for the sorption of Sr^{2+}, Eu^{3+}, and Pb^{2+} by RB.

Temp.,K	Q,mmol/g			b,L/mmol			R^2		
	Sr^{2+}	Eu^{3+}	Pb^{2+}	Sr^{2+}	Eu^{3+}	Pb^{2+}	Sr^{2+}	Eu^{3+}	Pb^{2+}
298	1.26	0.76	0.33	1.13	1.21	3.10	0.97	0.97	0.98
308	1.34	0.77	0.35	1.31	1.67	3.26	0.98	0.98	0.97
318	1.36	0.81	0.37	1.63	1.84	3.86	0.99	0.97	0.98
328	1.42	0.84	0.38	1.81	2.22	4.16	0.97	0.97	0.98

ues of R^2 were attained ($R^2 > 0.99$), as listed in Table 1, and the values of $q_{e(Calc)}$ are more similar to the experimental values, $q_{e(Exp.)}$. As a result, chemisorption, a pseudo-second-order sorption mechanism, is the dominant mechanism (Hassan et al., 2020).

3.8. Equilibrium isotherm studies

The impact of ion concentration was examined in the 5×10^{-5}–2.5×10^{-2} mol/L range at pH 5.0, 0.1 g of sorbent dose, and altered temperatures. Fig. 10 displays that at low concentrations, the amount of sorbed ions onto RB rapidly increases. This is attributable to the existence of several active sites that eventually get saturated. The following formula was used to determine RB's capacity using the Langmuir isotherm.

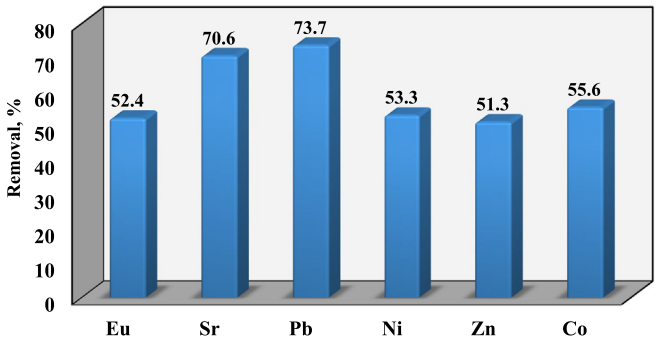

Fig. 11. Applying of RB on removal of altered ions from multicomponent system.

$$\frac{C_e}{q_e} = \frac{1}{bQ} + \frac{1}{Q}C_e \quad (6)$$

where b is the Langmuir constant associated with the sorption free energy and Q is the maximal capacity giving complete monolayer (mmol/g). Straight lines were gained when C_e/q_e was plotted against C_e, as explored in Fig. S2 (Supplementary Material). Q and b, respectively, are computed from the slope and intercept. According to Table 2, the capacity increased as the temperature rose. This demonstrates the endothermic character of the sorption process. The Q values are 1.26, 0.76, and 0.33 mmol/g at room temperature for Sr^{2+}, Eu^{3+}, and Pb^{2+}, respectively. The findings establish that Langmuir model efficiently agrees with the sorption data.

Additionally, RB used the Freundlich isotherm to solubilize Sr^{2+}, Eu^{3+}, and Pb^{2+}. The log q_e against log C_e plot gave scattered points, demonstrating that the model is inappropriate for the sorption of the three ions onto RB. The figures were omitted.

3.9. Application of RB on simulated radioactive waste

It was evaluated if RB biosorbent could effectively applied to remove different radionuclide-containing solutions. The RB was successfully applied to remove Sr^{2+}, Eu^{3+}, Pb^{2+}, Cs^{+}, Zn^{2+}, Co^{2+}, and Ni^{2+} from multicomponent solution, as simulated waste. The use of RB has demonstrated the efficient removal of the contaminants from the waste sample with percent removal ranging from 51.3 to 73.7%, as given in Fig. 11. The data established that RB can be applied successfully as a promising biosorbent for wastewater treatment.

Table 3
Comparing sorption capacity of Sr^{2+}, Eu^{3+}, and Pb^{2+} on natural and synthetic sorbents.

Sorbents	Experimental conditions	Capacity, mmol/g			References
		Sr^{2+}	Eu^{3+}	Pb^{2+}	
RB	pH = 5.0	1.26	0.76	0.33	Present work
Rice husks	pH = 5.0	* NR	* NR	0.55	(Johaiven et al., 2018)
Anadara inaequivalvis shell	pH = 4.0	* NR	* NR	0.03	(Bozbas and Boz, 2016)
Tomato waste	pH = 4.0	* NR	* NR	0.70	(Heraldy et al., 2018)
Hydroxyapatite-alginate nanocomposite	pH = 5.0	* NR	* NR	2.97	(Sangeetha et al., 2018)
Polyacrylonitrile/Na-Y-zeolite	pH = 3.0	* NR	* NR	0.36	(Elwakeel et al., 2018)
Mesoporous manganese oxide	pH = 5.7	0.29–0.39	NR*	NR*	(Ivanets et al., 2014)
Ti-Ca-Mg phosphates	pH = 6.0	1.98	NR*	NR*	(Maslova et al., 2019)
phosphatized dolomite (NaH_2PO_4)	NR*	2.5	NR*	0.6	(Ivanets et al., 2016)
granular activated carbon	pH = 10.0	0.25	* NR	* NR	(Sayed et al., 2022)
Roasted date pits	pH = 5.0	0.26	* NR	* NR	(Al-Absi et al., 2023)
PSS(AO-DAB18C6)	pH = 4.0	0.27	* NR	* NR	(Hamed et al., 2022)
Titanium phosphate	pH = 5.0	4.10	* NR	* NR	(Meng et al., 2023)
Tin(IV) vanadate	pH = 6.0	0.52	* NR	* NR	Abass et al., 2022
Kaolinite	pH = 5.0	NR*	0.09	NR*	(Kautenburger and Beck, 2010)
ZrFePH	pH = 4.0	NR*	0.22	NR*	(Misaelides et al., 2006)
Acetylacetone-modified silica gel	pH = 6.0	NR*	0.16	NR*	(Zhang et al., 2007)
GMZ bentonite	pH = 4.2	NR*	0.27	NR*	(Chen et al., 2012)
Resorcinol-formaldehyde Polymer	pH = 3.0	NR*	0.48	NR*	(Attallah et al., 2014)

*NR refers to Not Reported.

3.10. Comparing the obtained sorption capacity with altered sorbents

Table 3 reports a comparison of sorption capacities of Sr^{2+}, Eu^{3+}, and Pb^{2+} onto various sorbents gleaned from the literature. The different sorption capacities are ascribed to each sorbent's unique functional groups, surface area, and structural characteristics. Compared to many other sorbents, the value of the capacity exposed in this study is larger. It demonstrates that RB is viewed as an effective material for the sorption of Sr^{2+}, Eu^{3+}, and Pb^{2+}.

4. Conclusion

Sr^{2+}, Eu^{3+}, and Pb^{2+} are satisfactorily removed from the aqueous phase using the modified rice bran as a solid waste. According to calculations, the percentage elimination was 89.2, 81.4, and 80.5%, respectively, at the optimum conditions (pH = 5, equilibrium time = 90 min, particle size < 45 μm, metal ion concentration = 10^{-3}mol/L, and V/m = 10/0.1 mL/g). Ion exchange is used to carry out the sorption, and this process is managed by a pseudo-second-order mechanism. With monolayer capacities of 1.26, 0.76, and 0.33 mmol/g for Sr^{2+}, Eu^{3+}, and Pb^{2+}, respectively, the Langmuir sorption isotherm is applicable. The effectiveness of RB's sorption on a simulated radioactive waste was assessed; the outcomes showed that RB is a promising material for the treatment of liquid waste.

CRediT authorship contribution statement

Sayed S. Metwally: Conceptualization, Methodology, Writing – original draft, Writing – review & editing, Data curation, Project administration. **Emad H. Borai:** Visualization, Formal analysis, Writing – review & editing, Supervision. **Mostafa M. Hamed:** Validation. **Tarek M. Mohamed:** Resources. **Mahmoud G. Hamed:** Investigation, Data curation, Formal analysis. **Walaa R. Mohamed:** Investigation, Software.

Declaration of Competing Interest

The authors declare that they have no known competing financial interests or personal relationships that could have appeared to influence the work reported in this paper.

Acknowledgement

This paper is based upon work supported by Science, Technology & Innovation Funding Authority (STDF) under grant number 46016.

Appendix A. Supplementary material

Supplementary data to this article can be found online at https://doi.org/10.1016/j.arabjc.2023.105254.

References

Abass, M.R., Breky, M.M.E., Maree, R.M., 2022. Removal of 137Cs and 90Sr from simulated low-level radioactive waste using tin(IV) vanadate sorbent and its potential hazardous parameters. Appl. Radiat. Isotopes. 189, 110417.

Ahmed, I.M., Hamed, M.M., Metwally, S.S., 2020. Experimental and mathematical modeling of Cr(VI) removal using nano-magnetic Fe3O4-coated perlite from the liquid phase. Chinese J. Chem. Eng. 28 (6), 1582–1590.

Al-Absi, R.S., Khan, M., Abu-Dieyeh, M.H., Ben-Hamadou, R., Nasser, M.S., Al-Ghouti, M.A., 2023. The recovery of strontium ions from seawater reverse osmosis brine using novel composite materials of ferrocyanides modified roasted date pits. Chemosphere 311, (2) 137043.

Attallah, M.F., Borai, E.H., Shady, S.A., 2014. Kinetic investigation for sorption of europium and samarium from aqueous solution using resorcinol-formaldehyde Polymeric resin. J. Radioanal. Nucl. Chem. 299, 1927–1933.

Bozbas, S.K., Boz, Y., 2016. Low-cost biosorbent: Anadara inaequivalvis shells for removal of Pb(II) and Cu(II) from aqueous solution, Process Saf. Environ. 103, 144–152.

Chen, Y., Zhu, B., Wu, D., Wang, Q., Yang, Y., Ye, W., Guo, J., 2012. Eu(III) adsorption using di(2-thylhexly) phosphoric acid-immobilized magnetic GMZ bentonite. Chem. Eng. J. 181, 387–396.

El-Masry, E.H., Mohamed, T.M., Metwally, S.S., 2023. Post-irradiation physicochemical features of polymer composite for the removal of Co(II) and Nd(III) from aqueous solutions. Environ. Sci. Pollut. Res. 30, 11661–11674.

Elwakeel, K.Z., El-Bindary, A.A., Kouta, E.Y., Guibal, E., 2018. Functionalization of polyacrylonitrile/Na-Y-zeolite composite with amidoxime groups for the sorption of Cu(II), Cd(II) and Pb(II) metal ions. Chem. Eng. J. 332, 727–736.

Elwakeel, K.Z., Hamza, M.F., Guibal, E., 2021. Effect of agitation mode (mechanical, ultrasound and microwave) on uranium sorption using amine- and dithizone-functionalized magnetic chitosan hybrid materials. Chem. Eng. J. 411, 128553.

Ghaly, M., El-Sherief, E.A., Metwally, S.S., Saad, E.A., 2018. Utilization of nano-cryptomelane for the removal of cobalt, cesium and lead ions from multicomponent system: Kinetic and equilibrium studies. J. Hazard. Mater. 352, 1–16.

Hamed, M.M., Ahmed, I.M., Holiel, M., 2019a. Ahmed. Retention behavior of anionic radionuclides using metal hydroxide sludge. Radiochim. Acta 107, 1161–1172.

Hamed, M.G., El-Dessouky, S.I., Borai, E.H., 2022. Utilization of modified polymeric composite supported crown ether for selective sorption and separation of various beta emitting radionuclides in simulated waste. J. Molec. Liq. 353, 118799.

Hamed, M.M., Hassan, R.S., Metwally, S.S., 2019b. Retardation behavior of alum industrial waste for cationic and anionic radionuclides. Process Saf. Environ. Prot. 124, 31–38.

Hassan, H.S., Abdel Maksoud, M.I.A., Attia, L.A., 2020. Assessment of zinc ferrite nanocrystals for removal of 134Cs and 152+154Eu radionuclides from nitric acid solution. J. Mater. Sci. Mater. Electron. 31, 1616–1633.

Heraldy, E., Wahyu Lestari, W., Permatasari, D., Dwi Arimurti, D., 2018. Biosorbent from tomato waste and apple juice residue for lead removal. J. Environ. Chem. Eng. 6, 1201–1208.

IAEA, 2009. Controlling of degradation effects in radiation processing of polymers, Printed by the IAEA in Austria May 2009.

Ibrahim, H.A., Metwally, S.S., Mohamed, W.R., El-Sherief, E.A., Mekhamer, H.S., Moustafa, I.M.I., Mabrouk, E.M., 2021. Performance evaluation of fixed bed column packed with ionic liquid impregnated silica for separation of gadolinium and neodymium from aqueous solutions. Chromatographia 84, 335–345.

Ivanets, A., Kitikova, N., Shashkova, I., Matrunchik, Y., Kul'bitskaya, L., Sillanpää, M., 2016. Non-acidic synthesis of phosphatized dolomite and its sorption behaviour towards Pb^{2+}, Zn^{2+}, Cu^{2+}, Cd^{2+}, Ni^{2+}, Sr^{2+} and Co^{2+} ions in multicomponent aqueous solution Environ. Technol. Innovat. 6, 152–164.

Ivanets, A., Milyutin, V., Shashkova, I., Kitikova, N., Nekrasova, N., Radkevich, A., 2020. Sorption of stable and radioactive Cs(I), Sr(II), Co(II) ions on Ti–Ca–Mg phosphates. J. Radioanal. Nucl. Chem.

Ivanets, A.I., Shashkova, I.L., Kitikova, N.V., Drozdova, N.V., Saprunova, N.A., Radkevich, A.V., Kul'bitskaya, L.V., 2014. Sorption of Strontium Ions from Solutions onto Calcium and Magnesium Phosphates. Radiochem. 56, 32–37.

Kautenburger, R., Beck, H.P., 2010. Influence of geochemical parameters on the sorption and desorption behavior of europium and gadolinium onto kaolinite. J. Environ. Monit. 12, 1295–1301.

Kitikova, N.V., Ivanets, A.I., Shashkova, I.L., Radkevich, A.V., Shemet, L.V., Kul'bitskaya, L.V., Sillanpäa, M., 2017. Batch study of ^{85}Sr adsorption from synthetic seawater solutions using phosphate sorbents. J. Radioanal. Nucl. Chem. 314, 2437–2447.

Makarov, A.V., Safonov, A.V., Konevnik, Y.V., Teterin, Y.A., Maslakov, K.I., Teterin, A. Y., Karaseva, Y.Y., German, K.E., Zakharova, E.V., 2021. Activated carbon additives for technetium immobilization in bentonite-based engineered barriers for radioactive waste repositories. J. Hazard. Mater. 401, 123436.

Maslova, M., Mudruk, N., Ivanets, A., Shashkova, I., Kitikova, N., 2019. A novel sorbent based on Ti-Ca-Mg phosphates: synthesis, characterization, and sorption properties. Environ. Sci. Pollut. Res. 27, 3933–3949.

Meng, Y., Wang, Y., Ye, Z., Wang, N., He, C., Zhu, Y., Fujita, T., Hanyu, W.u., Wang, X., 2023. Three-dimension titanium phosphate aerogel for selective removal of radioactive strontium(II) from contaminated waters. J Environ. Manag. 325, 116424.

Metwally, S.S., Rizk, H.E., Gasser, M.S., 2017a. Biosorption of strontium ions fromaqueous solution using modified eggshell materials. Radiochim. Acta 105 (12), 1021–1031.

Metwally, S.S., Rizk, H.E., Gasser, M.S., 2017b. Biosorption of strontium ions from aqueous solution using modified eggshell materials. Radiochim. Acta 105 (12), 1021–1031.

Metwally, S.S., Hassan, R.S., El-Masry, E.H., Borai, E.H., 2018. Gamma-induced radiation polymerization of kaolin composite for sorption of lanthanum, europium and uranium ions from lowgrade monazite leachate. J. Radioanal. Nucl. Chem. 315, 39–49.

Misaelides, P., Sarri, S., Zamboulis, D., Gallios, G., Zhuravlev, I., Strelko, V.V., 2006. Separation of europium from aqueous solutions using Al3+ -and Fe3+ -doped zirconium and titanium phosphates. J. Radioanal. Nucl. Chem. 268, 53–58.

Mohamed, T.M., Attia, M.S., El-Sayyad, G.S., Fathy, R.M., El-Batal, A.I., 2022a. Gamma radiation crosslinking of PVA/myrrh resin thin film for improving the post-harvest time of lemon fruits. RSC Adv. 12 (9), 5619–5628.

Mohamed, W.R., Sami, N.M., Metwally, S.S., Saad, E.A., 2022b. Surface modification of ball clay minerals with gamma irradiation polymerization for removal of cerium and gadolinium ions from aqueous phase. Hydrometall. 208, 105816.
Montanher, S.F., Oliveira, E.A., Rollemberg, M.C., 2005. Removal of metal ions from aqueous solutions by sorption onto rice bran. J. Hazard. Mater. B117, 207–211.
Naga, A., Krishna Mohan, G.V., Kalpana, K., Ravindhranath, K., 2017. Removal of lead from water using calcium alginate beads doped with hydrazine sulphate-activated red mud as adsorbent. J Anal Method Chem 2017, 1–13.
Panasenko, A.E., Shichalin, O.O., Yarusova, S.B., Ivanets, A.I., Belov, A.A., Dran'kov, A. N., Azon, S.A., Fedorets, A.N., Yu Buravlev, I., Yu Mayorov, V., Kh Shlyk, D., Buravleva, A.A., Merkulov, E.B., Zarubina, N.V., Papynov, E.K., 2022. A novel approach for rice straw agricultural waste utilization: Synthesis of solid aluminosilicate matrices for cesium immobilization. Nucl. Eng. Technol. 54, 3250–3259.
Qinglan, W.u., Ren, M., Zhang, X., Li, C., Li, T., Yang, Z., Chen, Z., Wang, L.i., 2021. Comparison of Cd(II) adsorption properties onto cellulose, hemicellulose and lignin extracted from rice bran. LWT - Food Sci. Technol. 144, 111230.
Qu, J., Tian, X., Jiang, Z., Cao, B., Akindolie, M.S., Hu, Q., 2019. Multi-component adsorption of Pb(II), Cd(II) and Ni(II) onto microwave-functionalized cellulose: Kinetics, isotherms, thermodynamics, mechanisms and application for electroplating wastewater purification. J. Hazard. Mater. 387, 121718.
Rwiza, J.M., Seok-Young, O., Kyoung-Woong, K., Don Kim, S., 2018. Comparative sorption isotherms and removal studies for Pb(II) by physical and thermochemical modification of low-cost agro-wastes from Tanzania. Chemosphere 195, 135–145.
Sami, N.M., Elsayed, A.A., Ali, M.M.S., Metwally, S.S., 2022. Ni-alginate hydrogel beads for establishing breakthrough curves of lead ions removal from aqueous solutions. Environ. Sci. Pollut. Res. 29, 80716–80726.
Sangeetha, K., Vidhya, G., Girija, E.K., 2018. Lead and cadmium removal from single and binary metal ion solution by novel hydroxyapatite/alginate/gelatin Nanocomposites. J. Environ. Chem. Eng. 6, 1118–1126.
Shujun, Y., Huiyang, M., Chen, X., Tan, X., Ahmad, B., Alsaedi, A., Hayat, T., Wang, X., 2015. Impact of environmental conditions on the sorption behavior of radionuclide 90Sr(II) on Na-montmorillonite. J. Mol. Liq. 203, 39–46.
USEPA, 2012. Rare earth elements: a review of production, processing, recycling, and associated environmental issues. https://doi.org/EPA/600/R-12/5722012.
Wei, Y., Salih, K.A.M., Rabie, K., Elwakeel, K.Z., Zayed, Y.E., Hamza, M.F., Guibal, E., 2021. Development of phosphoryl-functionalized algal-PEI beads for the sorption of Nd(III) and Mo(VI) from aqueous solutions – Application for rare earth recovery from acid leachates. Chem. Eng. J. 412, 127399.
Weng, F.u., Deng, Y., Ram, R., Etschmann, B., Owen, N.D., Brugger, J., Vaughan, J., 2020. Selective removal of radioactive 210Pb(II) and nonradioactive Pb(II) isotopes from Cu(II)-rich acidic chloride solution by a new polyamine anion exchanger. Sep. Purif. Technol. 251, 117359.
Zhang, N., Huang, C., Hu, B., 2007. ICP-AES determination of trace rare earth elements in environmental and food samples by on-line separation and preconcentration with acetylacetone-modified silica gel using microcolumn. Anal. Sci. 23, 997–1002.
Zhao, G., Mengqi, H.u., Xiwen, L.u., Zhang, R., 2022. LWT Food Sci. Technol. 154, 112732.
Zhuang, X., Yin, T., Han, W., Zhang, X., 2019. Rice Bran and Rice Bran Oil: Chemistry, Processing and Utilization, 247–270.